Sum-frequency generation microscope for opaque and reflecting samples

D. M. P. Hoffmann, K. Kuhnke,[a] and K. Kern

Max Planck-Institut für Festkörperforschung, Heisenbergstr. 1, D-70569 Stuttgart, Germany

We report on the performance of a microscope setup, which has been developed for the imaging of sum-frequency generation (SFG) from reflecting, nontransparent samples. In order to maximize the SFG intensity the sample has to be observed from one side at an angle near 60° with respect to the surface normal. The setup is designed (a) to keep focus over the full image field and (b) to compensate for the distortion of the field-of-view, both by means of a blazed grating. In contrast to ''specular'' SFG spectroscopy, the incident beams reflected from the sample and the generated SF light cannot be separated by angular filtering. In this setup the separation thus relies on spectral filtering only. © *2002 American Institute of Physics.* [DOI: 10.1063/1.1499757]

I. INTRODUCTION

Nonlinear optics comprises a number of powerful techniques in material analysis and much effort is presently made to develop imaging methods that combine high spatial resolution with the specific properties of various nonlinear optical processes. Examples for recent efforts are improvements in coherent anti-Stokes Raman spectroscopy (CARS) microscopy,[1] the increasing number of second harmonic generation microscopes all over the world, the construction of the first sum-frequency microscope,[2] and first results in combining near field techniques with sum-frequency generation.[3–5] One basic advantage of processes, which involve more than one incident photon, is the fact that the spatial resolution can be improved when compared with an equivalent linear process.[6,7] In addition, high interface specificity can be obtained for second order optical processes, e.g., nonlinear processes such as second harmonic generation (SHG) and sum-frequency generation (SFG).

In a SFG experiment, two intense light pulses are overlapped on a sample in time and space to generate light at the sum of the frequencies of the two light waves. In the electric dipole approximation, the generation is absolutely interface specific for centrosymmetric samples. Even for noncentrosymmetric samples, the method has been shown to remain interface sensitive. Due to its nonlinearity, the process shows low efficiency and the incident beams have to be focused to get close to the corresponding sample damage threshold in order to minimize measuring times. In a SHG experiment, only one intense beam is incident on the sample and the doubled frequency is observed. Whereas the SHG signal for wavelengths typically shorter than 1 μm is often determined by electronic transitions at the sample, the use of SFG with an infrared (IR) and a visible beam allows vibrational spectroscopy in the IR thus obtaining chemical contrast from vibrational transitions.

SHG microscopy has been developed as a scanning method to study biological tissues[8] and sample inhomogeneities. Further it was developed instrumentally to study the one-dimensional diffusion of metals on metals[9] and became a full interface imaging technique.[10] Similar to CARS microscopy and in contrast to IR microspectroscopy, both lateral resolution limit and detection efficiency of SFG microscopy (SFM) are due to the generated visible wavelength (e.g., around 450 nm) although it is sensitive to transitions, which correspond to wavelengths of several micrometers. It has been shown that in SFM, areas of different chemical composition or varying molecular orientation can exhibit contrast at characteristic IR wavelengths.[11] SFM thus combines in one instrument potential μm spatial resolution, sensitivity to even buried interfaces, chemical contrast, and—depending on the time structure of the employed incident beams—ns or ps time resolution.

In the literature, there are some promising first results in near-field SFG microscopy. Still, we decided to build a far-field SFG microscope for several reasons: The SFG intensity of interfaces or even submonolayers is generally very low, thus demanding integration over several laser shots. Taking images of larger areas (e.g., 100×100 pixels) by means of scanning will thus require long measuring times. Given the limit of surface damage, which restricts the power per surface area for the incident beams, lasers with low repetition rate (20 Hz) and high pulse energy (>100 μJ) such as the one we use in our laboratory, make it far more preferable to measure those pixels simultaneously and not in a pointwise scanning mode. Moreover, the quantitative interpretation of data becomes much more involved when near-field light sources or near-field detection are employed.

Although accessible by common laser equipment and in spite of its attractive properties, to our knowledge only one IR-vis-far-field SFG microscope (SFM) has been reported yet.[11] This may have to do with the low efficiency of the SFG process and the close angular and spectral proximity of the visible beam and the generated SFG beam. The solution to overcome this problem in the above-mentioned SFM setup is the use of total internal reflection in the substrate for the incident visible beam, a solution that limits, however, the

---

[a]Author to whom correspondence should be addressed; electronic mail: k.kuhnke@fkf.mpg.de
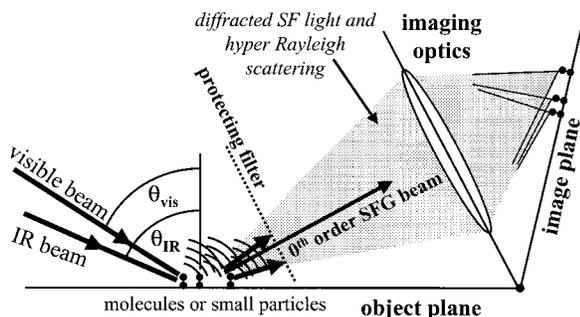
FIG. 1. Principle of SFG microscopy. In contrast to "classical" SFG spectroscopy not only the specular beam is observed. Diffracted beams contain the light emitted by pointlike sources and carry the information of sample inhomogeneities.
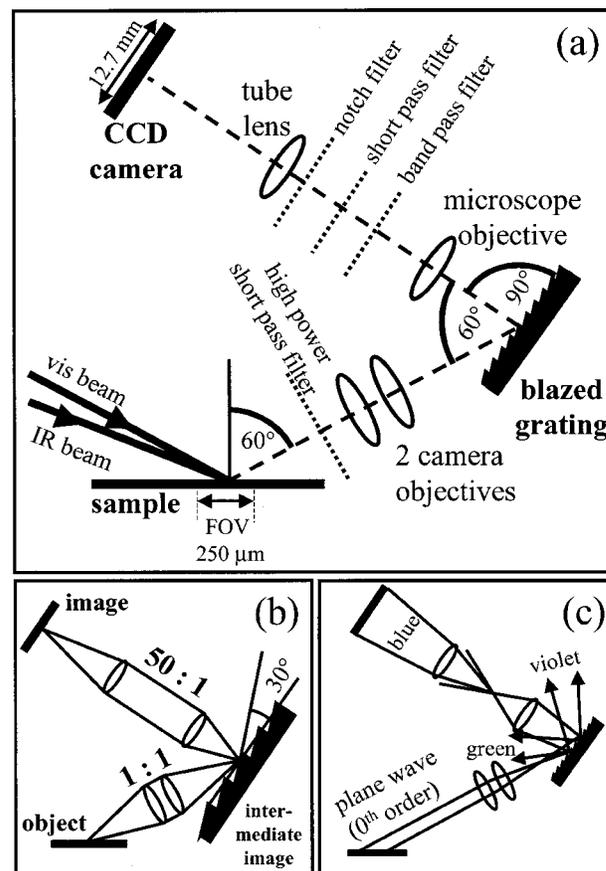

FIG. 2. (a) Schematic setup of the SFG microscope with the employed optical elements. (b) Path of the imaging beam. (c) Path of the illumination beam. FOV=field of view.

applicability to substrates which are transparent in the visible region and excludes the important classes of metals and semiconductors. For these reflecting substrates, the illumination has to be made from the observation side of the sample by oblique incidence in order to obtain a high electric field component at the surface (Fresnel factors). For oblique incident beams the most intense SFG component leaves the surface at a similarly large angle, which is determined by the two-dimensional wave vector conservation at a homogeneous interface.

Depending on incidence geometry and wavelengths, this SFG light is emitted in a direction at most a few degrees away from the reflection of the incoming visible beam. Emission from regions breaking the translational in-plane symmetry of a sample, however, does not obey wave vector conservation. SFG light of higher multipole order than electric dipole emission which can be emitted from small aggregates or SFG light carrying structural information from the sample (e.g., emitted near sample inhomogeneities) propagates in directions covering a large solid angle (Fig. 1). Sampling a substantial part of this light and obtaining full spatial information thus prohibits an angular separation of SFG light and reflected light from the incident beams which is usually the basis for background suppression in coherent, specular SFG spectroscopy at interfaces.

In this article, we describe a setup, which allows SFG microscopy to overcome the problems sketched above. A combination of four filters is employed to suppress the reflected beams, sample fluorescence, and background light. Detection via an intermediate image on the surface of a blazed grating allows distortion-free mapping and perfect focusing over the entire imaged area. The transmission of the setup is high enough for SFG spatially resolved spectroscopy. The setup can be used to image microstructures including biological samples with all the selectivity of IR-vis SFG spectroscopy. Different sample regions can be monitored simultaneously (combinatorial spectroscopy) allowing the mapping of inhomogeneities in chemical composition (e.g., phase boundaries) and imaging a varying degree of ordering. The microscope setup is an extension of conventional SFG spectroscopy, which facilitates addressing questions of sample inhomogeneity that had to remain unanswered in many SFG spectroscopic studies in the past.

II. DESIGN

The setup is sketched as a whole in Fig. 2(a). The essential components, charge-coupled device (CCD) camera, employed filters, and imaging via the blazed grating will be discussed in the following paragraphs.

We base our construction on the aim to observe the SFG signal from mixing a 532 nm visible light pulse (second harmonic generated by the 1064 nm pulses from a Nd:YAG laser with 35 ps pulse length and 20 Hz repetition rate) with IR light from a narrow band optical parametric generator and amplifier setup (similar to Ref. 12) covering the important region of vibrational transitions between 1000 and 4000 cm^{-1} (10–2.5 μm). Restricting ourselves to spectroscopy in the range of 2.9–4 μm, the SFG signal will have a wavelength between 450 and 470 nm. The setup can in principle be extended to a larger IR region and also allows difference frequency generation for the same IR range after exchanging some of the spectral filters and the grating.

The energy of the 35 ps laser pulses employed for the SFG measurements in this article are 200 μJ/pulse in the visible beam at 532 nm slightly focused to a large spot of 4 mm^2 and 250 μJ/pulse in the IR pulse at 3.45 μm (2900 cm^{-1}) focused to about 0.1 mm^2.

The desire for high quantum efficiency for photon detection and low noise led to the choice of a back-thinned, liquid-N_2 cooled CCD camera. We use a grade 1 SITe chip

with 512×512 pixels of $(24 \; \mu m)^2$ area each, integrated in a camera built by Roper Scientific. In this article we present only measurements made directly with this CCD detector, although we can alternatively mount a gated intensifier onto this camera.

In order to use optimal instrumental resolution, the pixel size should be at least two times smaller than the limit given by the imaging optics (Nyquist theorem). Depending on the objectives used, one may expect a resolution down to 1 μm. We thus chose a magnification factor of 50 so that one pixel represents an area of $(0.5 \; \mu m)^2$ on the sample. The total field of view seen by the CCD is $(250 \; \mu m)^2$ which is adequate to many types of interface studies. Further magnification will be disadvantageous given the operational limitation by sample damage that sets a limit to the absolute number of photons, which can be emitted for a given sample, surface area, and pulse duration. A number for our experimental conditions will be given below.

The intense visible and IR beams incident on the sample in a SFG experiment are, to a substantial percentage, reflected from a metallic or semiconducting sample. It is generally not difficult to attenuate the mid-IR beam (3–10 μm) because most optical components in a microscope have a vanishing transmission in this range. In contrast, one cannot avoid the fact that the reflected beam at 532 nm will exhibit a tight focus within the glass components of the objectives and can thus easily damage the imaging optics. One can estimate that an attenuation of >4 orders of magnitude for this beam is necessary already in front of the first objective. In our setup this is done by a low-cost dichroic short pass interference filter (edge 460 nm; Linos Photonics) which itself is not damaged by the intense visible beam and transmits $>80\%$ of the SFG signal.

Reflecting samples have to be illuminated by visible and IR light at incidence angles around 60° with respect to the interface normal in order to maximize the Fresnel factor and thus the SFG intensity for the important *ppp* polarization combination, i.e., when incident and SFG beams are all *p*-polarized. It follows that the zeroth order coherent SFG beam also leaves at angles near 60° in a direction close to the reflected visible beam. This means that this most intense SFG beam will hit the entrance lens of a conventional optical microscope observing the sample along the surface normal only close to the lens edge. At the same time the objective will obstruct the incoming visible and IR beams. Aligning the imaging optics along the axis of the zeroth order SFG signal, however, will yield a focus only along one line while sample regions in front of or behind the focal plane will be out of focus on the CCD camera. A hypothetical solution to solve these two problems would be the use of a sample with a zigzag surface similar to a grating with a blaze angle of 30° and facets of $<1 \; \mu m$ height. From each facet the SFG zeroth order light is emitted right into the objective, which is observing the grating from above while the whole surface stays within the depth of focus of the objective. Of course, such a concept would impose unacceptable restrictions on sample geometry. The principle, however, can be developed further in the following way: light originating from a flat surface or interface is projected without magnification onto a blazed grating [see imaging path in Fig. 2(b)]. This image is then magnified by a microscope whose axis is perpendicular to the macroscopic surface of the grating. The grating thus has to be placed in the image plane of the nonmagnifying 1:1 system as well as in the object plane of the $50\times$ microscope system. Its blaze angle is 30° so that the light emitted from one point of the sample is reflected into the microscope objective [Fig. 2(b)]. In addition, its grating constant must be such that SFG light from the surface is diffracted in first order by the grating towards the microscope objective [illumination path in Fig. 2(c)]. For a 450 nm SFG wavelength, we chose a 1800 lines/mm (blaze 500 nm) grating (supplier Jobin–Yvon). For the 1:1 imaging of the sample onto the grating, we use two $f = 58$ mm, $f/1.2$ Noct–Nikkor objectives with aspherical lenses. The $50\times$ microscope consists of an LPlan 50×0.45 objective (Nikon) with 17 mm working distance and a tube lens. Apart from keeping perfect focus, our setup has another important property, namely, that the image of a sample appears on the CCD as if the sample is directly observed from above, i.e., a square on the sample becomes a square in the image. It allows obtaining undistorted images in spite of observation from the side. After having developed and tested the design, we became aware of a proceedings contribution by Chastang[13] published in 1983 which analyzes the properties of oblique imaging via a grating and proposes the scheme as a microscope attachment. We could not find a publication on an application of this scheme.

The suppression of stray light from various sources is an important point given the small intensity of the SFG signal. As a general measure, the whole setup is covered by a box made of black cardboard, which admits light only along the imaging beam path. Apart from diffuse light originating from room illumination, sample luminescence and especially the reflected visible beam must be attenuated by several orders of magnitude in order to become negligible with respect to the SFG signal. A basic attenuation along the beam path is obtained by a holographic notch filter (center 532 nm, width 10 nm; Kaiser Optical Systems Inc.), which removes almost 5 orders of magnitude of the visible beam while letting 70% of the SFG signal pass. The combination of a bandpass filter (450 nm, width 40 nm; L.O.T.-Oriel) and a short pass filter (edge 510 nm, Omega Optical Inc.) suppresses in addition both shorter wavelengths from ambient light and longer wavelengths, which may be efficiently generated by luminescence of the sample. These interference filters are inserted in-between the microscope objective and the tube lens, where all light beams propagate at a minimum angle with respect to the optical axis [Fig. 2(a)]. The effective wavelength-dependent transmission of the combination of the 4 filters discussed above is shown in Fig. 3 for the sensitive spectral range of the CCD camera. The visible incident beam at 532 nm is suppressed by more than 20 orders of magnitude while about 30% of the SFG signal near 450 nm is transmitted. An additional significant attenuation of wavelengths longer or shorter than the SFG signal is due to the blazed grating [Fig. 2(c)].

If required for certain cases, our setup can be turned into the setup of specular SFG spectroscopy without sacrifice of sensitivity by complete binning of the image and replacing
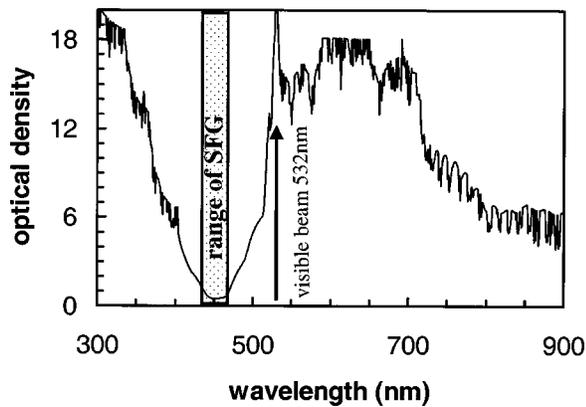
FIG. 3. Synthetic absorption curve of the four-filter-combination discussed in the text. The curve is the product of four absorbance curves measured for the individual filters. Due to the limited sensitivity of the spectrometer optical densities larger than five may be underestimated in this plot and may in reality be larger.

the first filter between sample and objective by a pinhole that selects only the specular SFG beam by angular filtering.

III. EVALUATING IMAGES OF TEST STRUCTURES

The properties discussed in the following paragraphs are not essentially different for linear and nonlinear optics but they are obtained much faster in linear optical experiments. We thus chose to characterize the optical system by linear optics and imaged calibrated test structures (NBS test No. 29, supplier: Heidenhain) in transmission employing narrow band blue incoherent light.

An omnipresent and rather trivial reduction of image quality is due to localized flaws in spectroscopic filters, grating inhomogeneities, and, finally, small dust particles on different optical components in the beam path. For linear optics imaging, Fig. 4 shows that most of these spots can be removed by dividing the image by an average of some 20 images taken on different parts of a homogeneous and unstructured sample. This type of general flat field correction by an average of linear optical images has been applied to all linear images and the SFG images in Fig. 8. A second problem arises specifically at extremely low light levels, as in SFG imaging: the number of cosmic ray events in an exposure can become important for exposure times of several minutes. Each such event affects mostly 2, rarely up to 4 pixels [see, e.g., Fig. 7(b)] and is stochastic in the sense that it affects different pixels in successive exposures. The spuri-

FIG. 5. Determination of image distortion. Top: image of a 22 linepairs/mm structure (a) for horizontal lines; (b) for vertical lines. Bottom: values obtained by evaluating the magnification in different parts of the images (c) for the vertical magnification; (d) for the horizontal magnification. The magnification values are printed in the region of the box equivalent to the region where they have been obtained in images (a) and (b).

ous count rates can thus be removed simply by comparison within a series of exposures under the same conditions.

Figure 5(a) shows horizontal lines of a 22 linepairs/mm structure. The image allows evaluating the magnification in the vertical direction in several regions of the image field assuming a pixel distance of precisely 24 μm. The result is displayed in Fig. 5(c). In this figure the magnification values are printed in the region equivalent to the region where they have been obtained in the original image [Fig. 5(a)]. Equivalently, the vertical lines in Fig. 5(b) are used to obtain the magnification in the horizontal direction [Fig. 5(d)]. This evaluation yields an average vertical magnification factor of 50.3 ($\pm$0.5) and a horizontal magnification factor of 51.1 ($\pm$0.5). We give the error corresponding to an uncertainty of

FIG. 6. (a) Well-resolved test pattern (110 linepairs/mm); (b) resolution limit for vertical lines: 180 line pairs/mm; (c) for horizontal lines: 320 line pairs/mm.
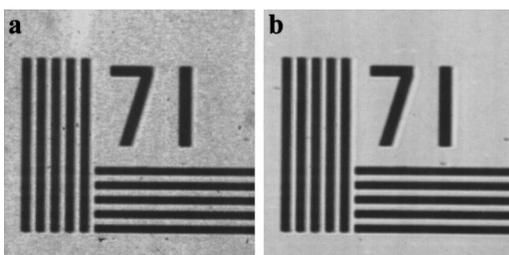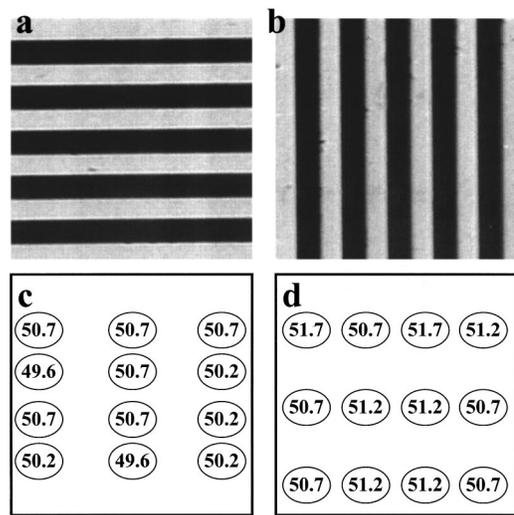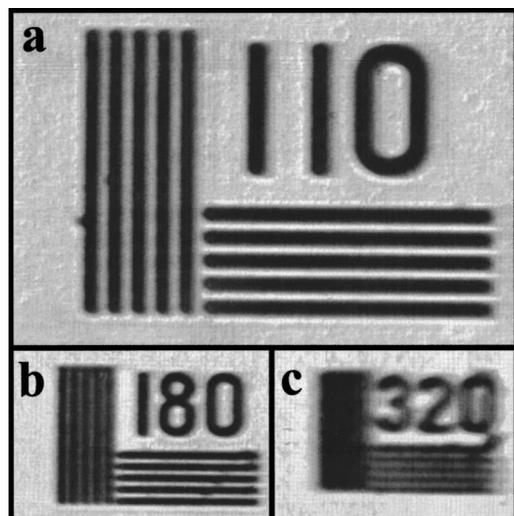

FIG. 4. Examples of the reduction of grating and filter inhomogeneities: (a) raw image; (b) the same image after normalization to an average of blank images (also see the text).

one pixel. Within this precision, we can say that we have distortion-free imaging.

Figures 5(a) and 5(b) also show that the edges of the stripes stay focused in the entire image and do not become blurred with increasing distance from the image center. This fact is nontrivial for the horizontal direction because the left edge of the images is 208 μm closer to the objective than the right edge. For comparison, focusing is done by approaching the sample to the first objective and must be done with <3 μm precision.

Figure 6(a) shows an image of a test structure with 110 linepairs/mm, which are still well resolved. Analyzing the images of still smaller structures allows us to find the resolution limit. We verified by numerical convolution that the resolution defined by the Rayleigh criterion is given by the period of the striped structure which exhibits 8% of the intensity modulation of a perfectly well resolved structure (see also Ref. 14). By interpolating a series of images for different stripe periods we find that this limit is reached for the horizontal resolution at 4.9 μm [approximately the period of vertical stripes in Fig. 6(b)] and for the vertical resolution at 2.8 μm [approximately the period of horizontal stripes in Fig. 6(c)]. In experimental practice it should often be possible to rotate the sample in a way to make use of the better resolution.

The anisotropic resolution is a consequence of oblique imaging. It results from the fact that a square on the sample appears as a rectangle when we watch from the direction of the first objective. The apparently shorter distance in the square creates a diffraction pattern, which leads to beams under larger angles than the apparently longer distance. It is for this reason that the camera objective, which lets pass a circular section in reciprocal space, can still transmit the first order diffraction of the apparently larger distance while it already misses the first order of the apparently shorter distance. From this reciprocal space argument we expect the ratio between vertical and horizontal resolution to be $\cos(60°)=0.5$ in reasonable agreement with our result. This argument is valid for diffraction-limited imaging but the corresponding argument holds if the resolution is limited by spherical aberration errors.

The diffraction limited resolution at $\lambda=450$ nm derived from the Abbe formula $\Delta x=1.22*\lambda/NA$, in which NA is the numerical aperture, is $\Delta x=0.92$ μm for the camera objectives (NA=0.6) and $\Delta x=1.22$ μm for the microscope objective (NA=0.45). We find that our result for the resolution does not attain this limit. As an intermediate image is created on the grating the worse of the objectives will determine the overall resolution. Experiments in which we tested both systems separately showed clearly that the microscope objective almost reaches its diffraction limit while one single camera objective only attains a resolution of about 4 μm at $\lambda=632.8$ nm. This demonstrates that the resolution in the setup is due to the fact that the camera objectives do not reach the diffraction limit. This result might suggest that a substantially smaller aperture can be used for the 1:1 projection. The large aperture size is, however, useful in order to collect a maximum of light emitted from strongly inhomogeneous samples as we already discussed in the Introduction.
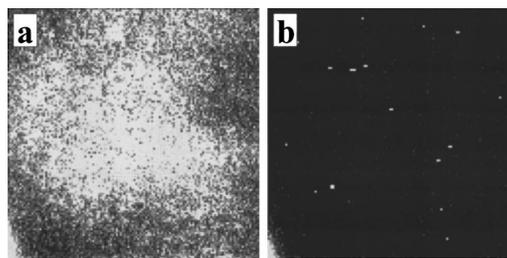

FIG. 7. Proof of background suppression: Uncorrected raw data with 5 min exposure time, 4×4 pixels binned. (a) SFG intensity from a GaAs sample; (b) same conditions but with the visible beam delayed by 50 ps with respect to the IR beam. The intensity scales for both images are identical. White pixels in (b) are due to cosmic rays. The bright spot in the lower left corner is due to an inhomogeneity of CCD dark current.

So far we characterized the optical performance of the microscope itself. In the remainder of this section we will demonstrate its performance for the SFG method. As we pointed out earlier the damage threshold of a sample ultimately limits its SFG photon yield. A good SFG microscope will detect a large amount of the generated photons. We will give integration times below this limit for the 35 ps 20 Hz laser pulses described in Sec. II. Pushing the damage threshold by using higher repetition rates and shorter pulses each containing less energy will reduce the necessary measuring times.

Figure 7(a) gives an example for the observation of a sum-frequency signal for the microscope setup with coincident 532 nm (visible) and 3.4 μm (IR) pulses. Both beams have to overlap in time and have to be adjusted to the sample area imaged by the microscope. The observed SFG signal generated by a GaAs sample corresponds to 3.4×10^6 photons detected by the CCD chip during an exposure of 300 s (6000 laser shots). The pixels were binned 4×4. The detected average intensity is thus 2.6 photons/min originating from a $(0.5 \mu m)^2$ area. The intensity in the center of Fig. 7(a) is 3.7 photons/min. We could not obtain higher intensities without damaging the GaAs sample. We remark that in the case of GaAs the observed SFG signal is dominated by the bulk contribution. The intensity distribution in the image is due to the visible and IR beam profiles. As expected for a SFG process, the observed intensity disappears completely when either the visible or the IR beam is blocked. Figure 7(b) proves furthermore that no light is observed when both beams are incident but the visible pulse is delayed by 50 ps with respect to the IR pulse (pulse length 35 ps). This demonstrates the absence of background and luminescence light in the image. We also want to give an estimate for the SFG signal obtainable for an octadecanethiolate monolayer on polycrystalline Au. This system exhibits a SFG signal arising exclusively from its surface and shows vibrational transitions in the IR region discussed here. For such a sample the spectroscopically relevant signal from the adlayer can become 30% of the total signal, which is dominated by the contribution of the Au surface. Due to its higher damage threshold for IR pulses such a sample allows to use a more tightly focused IR beam than a GaAs sample. Preliminary results show that we can easily obtain 1 photon/min/$(0.5 \mu m)^2$ area (10^6 photons per 300 s in the image) with our laser source.
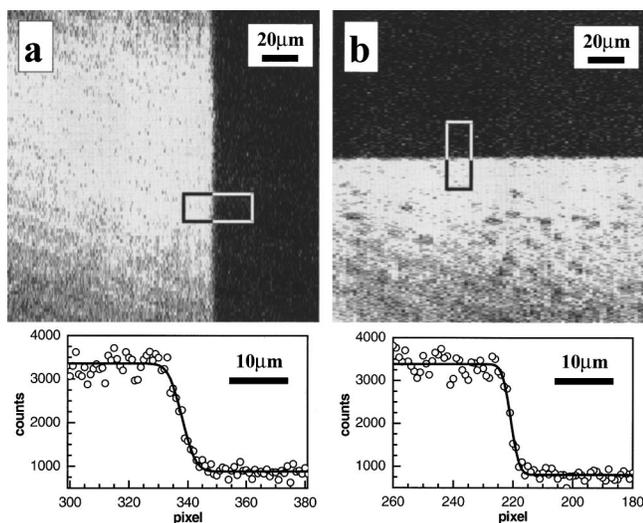
FIG. 8. Resolution in a SFG image: (a) for a vertical and (b) a horizontal edge of a GaAs sample. The exposure time was 120 min. In the measurements, four pixels parallel to the edge were binned keeping the resolution perpendicular to the edges. At the bottom the average of eight line scans in the boxed area are shown together with the fits discussed in the text.

This value was obtained still far from the IR damage threshold so that higher flux densities are obtainable and the signal from alkane-thiolate covered Au can become comparable to the one from GaAs. With our present IR beam we obtain higher SF fluxes only at the cost of nonuniform illumination of the field of view.

In order to verify the anisotropic resolution for oblique SFG imaging, we recorded images of the edges of a GaAs wafer broken along defined crystallographic directions. Such edges are known to be straight and sharp on a sub-μm scale. Already on first inspection of Fig. 8 the SFG image shows sharp imaging without signs of defocusing at the edges of the image field and a better resolution in the vertical than in the horizontal direction. In both measurements, four pixels were binned in a row parallel to the respective sample edge. As the edges are parallel to the rows of the pixels, this type of binning reduces the readout noise without reducing the resolution in the direction perpendicular to the respective edges. Fitting an error function (erf) to an average of 8 such line scans yields as a distance between the 10% and the 90% intensity level a value of 4.6 μm for the vertical and 2.9 μm for the horizontal edge. This corresponds to a resolution according to the Rayleigh criterion of 4.9 μm in horizontal and

3.1 μm in vertical direction, in good agreement with the above results obtained by the linear optics experiment.

IV. OUTLOOK

A substantial improvement should be possible by realizing a near diffraction limited 1:1 imaging system with high numerical aperture. To our knowledge, such a system is not commercially available and will have to be developed. A grating and spectral filters with lower defect density could reduce the flaws visible on the raw data. The use of an image intensifier in front of the CCD camera will help to eliminate readout noise substantially. This is the main source of noise in the images shown in this article. A gated intensifier relaxes the necessity to remove cosmic ray spikes and strongly reduces the sensitivity to background light, which is not synchronous with the laser pulses (e.g., ambient light) or which is delayed (luminescence). As a drawback it reduces the quantum efficiency for photon detection by almost an order of magnitude. Finally, the microscope that is presently mounted on a laser table shall be set up as a transportable unit, which also allows making measurements at different laser sources.

ACKNOWLEDGMENT

[1] A. Volkmer, J.-X. Cheng, and X. S. Xie, Phys. Rev. Lett. **87**, 23 901 (2001).
[2] M. Flörsheimer, C. Brillert, and H. Fuchs, Mater. Sci. Eng., C **8–9**, 335 (1999).
[3] Y. Shen, J. Swiatkiewicz, J. Winiarz, P. Markowicz, and P. N. Prasad, Appl. Phys. Lett. **77**, 2946 (2000).
[4] B. Humbert, J. Grausem, A. Burneau, M. Spajer, and A. Tadjeddine, Appl. Phys. Lett. **78**, 135 (2001).
[5] R. D. Schaller and J. Saykally, Langmuir **17**, 2055 (2001).
[6] J. Squier and M. Müller, Rev. Sci. Instrum. **72**, 2855 (2001).
[7] T. A. Klar and S. W. Hell, Opt. Lett. **24**, 954 (1999).
[8] I. Freund and M. Deutsch, Opt. Lett. **11**, 94 (1986).
[9] K. A. Schultz and E. G. Seebauer, J. Chem. Phys. **97**, 6958 (1992).
[10] M. Flörsheimer, D. H. Jundt, H. Looser, K. Sutter, M. Küpfer, and P. Günther, Ber. Bunsenges. Phys. Chem. **98**, 521 (1994).
[11] M. Flörsheimer, C. Brillert, and H. Fuchs, Langmuir **15**, 5437 (1999).
[12] H. J. Krause and W. Daum, Appl. Phys. B: Photophys. Laser Chem. **B56**, 8 (1993).
[13] J. C. Chastang, Proc. SPIE **399**, 239 (1983).
[14] W. J. Smith, *Practical Optical System Layout*, edited by F. R. E. and W. J. Smith, McGraw–Hill Optical and Electro-Optical Engineering Series (McGraw–Hill, New York, 1997).